Clays and Clay Minerals, Vol. 42, No. 3, 321–330, 1994.

TRANSFORMATIONS OF SYNTHETIC BIRNESSITE AS AFFECTED BY pH AND MANGANESE CONCENTRATION

SHIHUA TU, GEZA J. RACZ, AND TEE BOON GOH

Department of Soil Science, University of Manitoba Winnipeg
Manitoba, Canada R3T 2N2

Abstract—The amount of Mn^{2+} adsorbed or removed from solution by birnessite is several times greater than its reported cation exchange capacity. Extractability of the sorbed Mn^{2+} decreases with aging. It is uncertain whether the sorbed Mn^{2+} is oxidized on the surface or incorporated into the structure of birnessite. Using X-ray powder diffractometry and transmission electron microscopy, a study was conducted to examine the mineralogical alteration of birnessite after treatment with various concentrations of $MnSO_4$ and solution pH.

The sorbed Mn^{2+} was not directly oxidized and remained on the birnessite surface. The sorption of Mn^{2+} was followed by alteration of birnessite with the formation of new Mn minerals. The specific Mn minerals formed were governed by the pH of the reaction, and the rate of the transformation was determined by Mn^{2+} concentration and pH. Nsutite and ramsdellite were identified at pH 2.4, cryptomelane at pH 4, groutite at pH 6, and manganite at pH 8. Other Mn minerals formed at these and other pH levels could not be identified. As the concentration of Mn in the solution decreased, the time required to form new minerals from the birnessite increased. The newly formed phases were the result of structural conversion since dissolution of birnessite and reprecipitation of new phases were not observed.

Key Words—Birnessite, Manganese oxides, Mn^{2+} concentration, pH, Structural conversion, TEM, XRD.

INTRODUCTION

Birnessite, $(Na_{0.7}Ca_{0.3})Mn_7O_{14}\ 2.8\ H_2O$, is one of the most common Mn minerals in soils (McKenzie, 1989). It has a layer lattice structure, with high specific surface areas (50 to 300 $m^2\ g^{-1}$) (Healy *et al.*, 1966; McKenzie, 1980b) and the lowest point of zero charge (PZC), pH 1.5 to 2.5, among the known Mn minerals (McKenzie, 1981). Thus birnessite develops a high surface charge and large CECs (63 to 240 cmol(+) kg^{-1}) (McKenzie, 1981; Golden *et al.*, 1986) at pH values normally encountered in soils.

McKenzie (1980a) reported that Mn oxides have a much higher affinity for Mn^{2+} than for other divalent cations such as Ni^{2+} and Zn^{2+}. A study conducted by Tu (1993) with three clay minerals (vermiculite, montmorillonite, and kaolinite) and four oxides or hydroxides of Fe (hematite, goethite), Mn (birnessite), or Al (bauxite, a mixture of gibbsite, boehmite, and diaspore) showed that birnessite had the highest adsorption capacity for Mn in solution, retaining 3 to 30 times more Mn than the other adsorbents. Fendorf *et al.* (1993) showed that the sorption reaction of Mn^{2+} onto birnessite was very rapid and was completed in <1 s, with $>80\%$ of the Mn^{2+} being adsorbed within 200 ms.

The nature and fate of the Mn^{2+} retained by birnessite are not fully understood. Pankow and Morgan (1981) proposed that specific adsorption was responsible for the high affinity of Mn oxides for Mn^{2+}, similar to adsorption of other transition metal ions on oxide surfaces of Al and Fe. It was suggested that the sorbed Mn^{2+} on the surface of Mn oxides was oxidized to Mn^{4+} and the oxidation reaction was catalyzed by the oxide surface at which the Mn^{2+} and OH^- accumulated. Murray and Dillard (1979), using X-ray photoelectron spectroscopy, were unable to detect any Mn^{2+} on the surface of birnessite after adsorption of Mn^{2+}.

Hydrous Mn oxides are characterized by their poor crystallinity, structural defects, domain intergrowths, cation vacancies, and solid solutions (Davis and Kent, 1990). The Mn^{2+} initially sorbed on the surface may later become incorporated into the Mn oxide structure at sites of structural defects and cation vacancies and/or as a result of extensive substitution of Mn^{2+} and Mn^{3+} for Mn^{4+} (Krauskopf, 1972; McKenzie, 1989). Tu (1993) reported that the Mn^{2+} was retained in easily exchangeable as well as nonexchangeable forms when Mn^{2+} was reacted with birnessite for a short period of time. The exchangeable form then changed to a nonexchangeable form with time. However, it was not clear whether the Mn^{2+} ion was oxidized *in situ* at the adsorption site or incorporated into the crystal structure of birnessite. Furthermore, there is no information available whether the adsorbed Mn would cause any structural alteration of birnessite at different solution pHs. Therefore, the objective of this study was to study the effect of concentration of Mn and solution pH on the alteration of birnessite after adsorption of Mn.

MATERIALS AND METHODS

Preparation of birnessite

Birnessite was prepared according to the method developed by McKenzie (1971). One mole of concentrated HCl was added dropwise to a boiling solution of 0.5 mole of $KMnO_4$ in 1.25 liter H_2O with vigorous

stirring. After boiling for a further 10 min, the precipitate was filtered and washed on Whatman #42 filter paper under suction until free of purple coloration in the filtrate. The product was air-dried at room temperature and ground for use.

Reactions of Mn^{2+} with birnessite

Birnessite, 0.33 g in weight, was suspended in a 100 ml beaker containing 30 ml of $MnSO_4$ solution and pH of the suspension was adjusted to 2.4, 4, 5, 6, 7, or 8 by addition of dilute NaOH. The pH, when adjusted to a particular value, was continually adjusted to the desired pH during the first two hours of reaction. The concentration of $MnSO_4$ used was 0.33 mol liter^{-1} (1.0 mol liter^{-1} in ionic strength) except for the suspensions of pH 2.4 and 8 where 0, 0.0033, 0.033 and 0.33 mol liter^{-1} were used. In order to compare the effect of Mn with some other cations on the structural changes of birnessite, the birnessite was also suspended in 0.33 mol liter^{-1} $Ca(NO_3)_2$, $Cu(No_3)_2$, or 1.0 mol liter^{-1} KCl solution without pH adjustment. Birnessite was also suspended in water and the pH of the suspension was adjusted to 1.5 using dilute HNO_3 or 8.0 with dilute NaOH solution. After the first 2 h of reaction, the beakers were covered with parafilm, but aeration was allowed through pinholes on the cover. The suspensions stood at room temperature (21°C) for periods of two months and were stirred three times each day.

About 20 mg of sample was taken daily during the first week and every 2 to 5 days thereafter with a transfer pipette. The sample was washed in a cellulose nitrate membrane filter (pore size 0.025 μm) with about 30 ml of deionized water and then examined by X-ray diffraction (XRD). The structural change was deemed to have been completed when no further change was observed on examination by XRD. Samples were also taken from the treatment with 0.33 mol liter^{-1} $MnSO_4$ at pH 2.4, 4, and 6 after 1, 3, and 5 days, washed on Whatman #42 filter paper until free of sulfate, and then examined under the transmission electron microscope (TEM) to provide information on processes of mineral conversion. A sample taken from each of the final products was observed under TEM for its crystal morphology as well.

The powder samples of the final products were used for X-ray diffractometry. Step scan X-ray diffraction data were collected from 5°–75°2θ, using a step interval of 0.05°2θ and a counting time of 2 s/step, with a Philips automated diffractometer system PW1710. A PW1050 Bragg-Brentano goniometer equipped with incident- and diffracted-beam Soller slits, 1.0° divergence and anti-scatter slits, a 0.2 mm receiving slit and a curved graphite diffracted-beam monochromator was used. The normal focus Cu X-ray tube was operated at 40 kV and 40 mA, using a take-off angle of 6°. The step scan data were then converted to Siemens.RAW file format prior to being processed using Siemens DIFFRAC software. A peak search routine was run to generate a list of d-spacings and intensities (.DIF file) and then the pattern profiles were printed. The data files were then used with Fein-Marquart's μPDSM Search-Match software (PDF-2 on CD-ROM, Set 42) in an attempt to identify the phases present.

Transmission electron microscopic (TEM) examination was conducted using suspensions (0.01 to 0.05%) dried on Formvar (ethylenedichloride) support films, which was previously mounted on 300 mesh copper support grids and coated with carbon. Examination of the specimen was performed using a Phillips TEM 420 transmission electron microscope.

RESULTS

Effect of salts and pH on transformation of birnessite

Synthetic birnessite has major X-ray diffraction peaks near 0.727, 0.361, 0.246, 0.233, 0.204, 0.172, and 0.142 nm (McKenzie, 1989) and a layer lattice structure. The birnessite synthesized in this work, however, had only four major XRD peaks near 0.735, 0.366, 0.244, and 0.141 nm (Figure 3a), similar to the birnessites found in soils by other workers (Jones and Milne, 1956; Frondel *et al.*, 1960; Brown *et al.*, 1971; Koljonen *et al.*, 1976). Under a transmission electron microscope (Figure 1a), birnessite was observed as needles that were clustered into balls. No transformation of birnessite occurred in water suspensions at pH 1.5 or 8.0 or in the KCl, $Ca(NO_3)_2$, and $Cu(NO_3)_2$ solutions after one month of incubation, indicating that neither addition of H^+ or OH^- nor cations such as K^+, Ca^{2+}, and Cu^{2+} apart from Mn^{2+} were able to initiate transformation of the crystal structure of birnessite to other crystalline forms at room temperature in a relatively short period of time as seen by the persistence of the major XRD peaks (Figure 2).

→

Figure 1. Transmission electron micrographs showing a synthetic birnessite a) and newly formed Mn minerals (b–f) from birnessite after treatment with 0.33 mol liter^{-1} $MnSO_4$ solution at different pHs after 10 to 60 days aging: a) synthetic birnessite, balls of needles; b) pH 2.4 (not adjusted), fibrous crystals (F) of ramsdellite and shuttle-shaped crystals (SS) of ramsdellite; c) pH 4, lath-shaped crystals of cryptomelane (CR), moss-like crystals (M) and pseudo-hexagonal stacks (SS); d) pH 5, rod-shaped crystals (R) and hexagonal cones (HC); e) pH 6, hexagonal cones (HC) and parallel intergrowths of slat-shaped crystals (bundle of needles) (S); and f) pH 8, short rod-shaped crystals of manganite (SR) and long rod-shaped crystals of an unknown (LR).

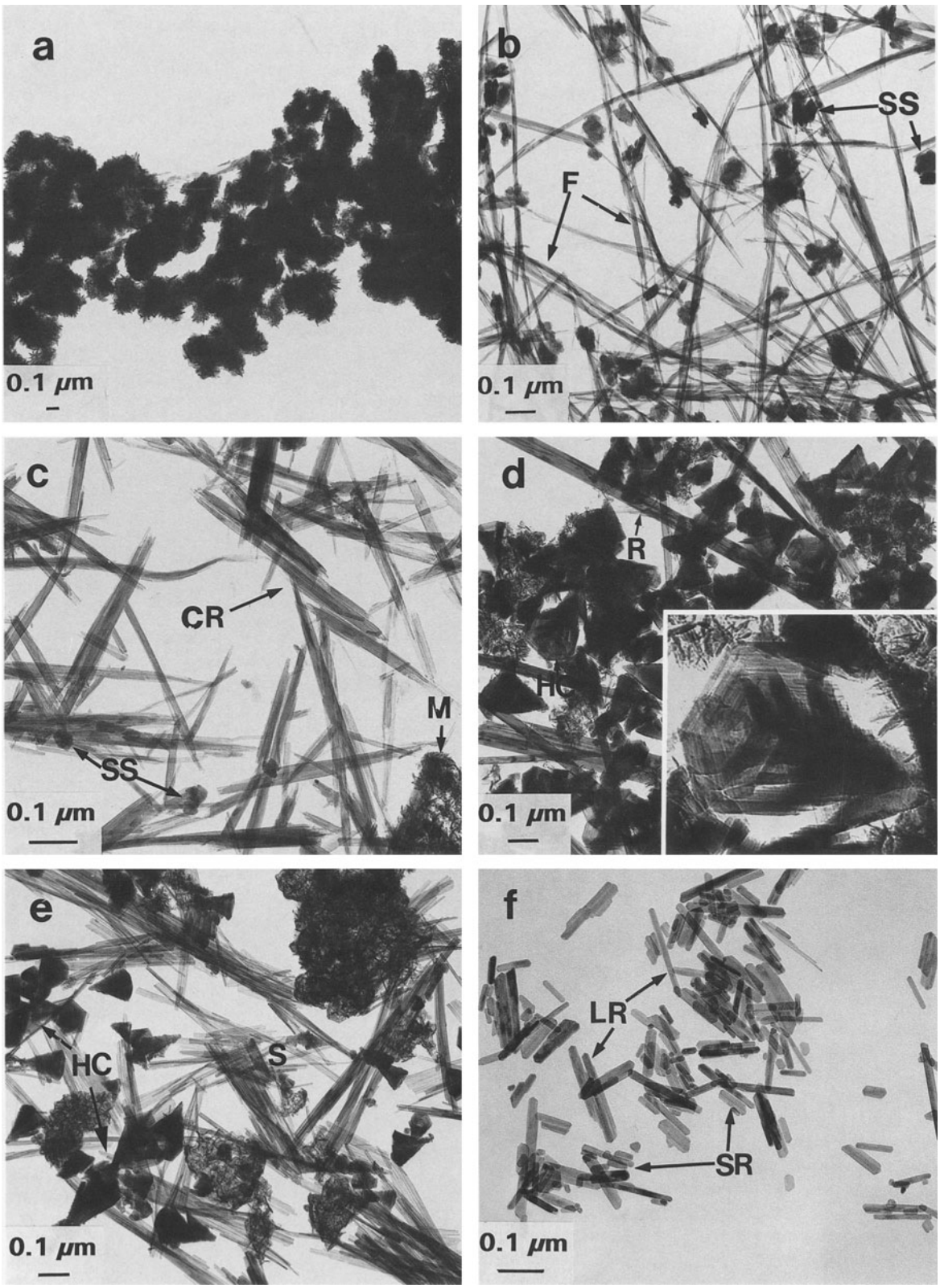

https://doi.org/10.1346/CCMN.1994.0420310 Published online by Cambridge University Press

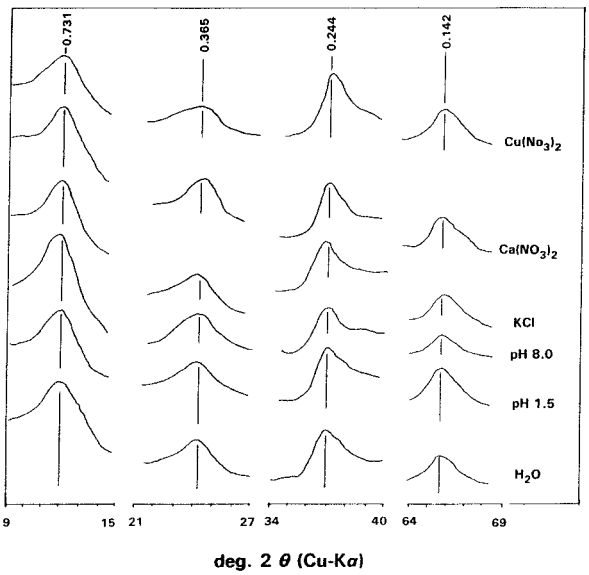

Figure 2. X-ray diffraction patterns of synthetic birnessite after aging in water at different pH and solution conditions.

Transformation of birnessite as affected by $MnSO_4$ at different pHs

When suspended in $MnSO_4$ solution, birnessite readily underwent mineralogical transformation at room temperature. The transformations observed were not only governed by pH but also by the concentration of Mn^{2+} of the mother liquor. The time required to complete transformation of birnessite varied with solution pH, ranging from 5 days for the treatment at pH 8 to 56 days for the treatment at pH 4. The original XRD peaks either disappeared or shifted after birnessite was suspended in the $MnSO_4$ solution (Figure 3 and Table 1). The XRD peaks indicated the formation of new Mn minerals. At a pH of about 2.4, two Mn minerals were identified from the XRD patterns: nsutite, a Mn oxide hydroxide, γ-$Mn(O, OH)_2$, where the Mn includes Mn^{2+}, Mn^{3+} and Mn^{4+} (McKenzie, 1989), with peaks positioned at 0.400, 0.259, 0.242, 0.233, 0.221, 0.213, 0.207, 0.190, 0.164, 0.148, 0.1424, and 0.1367 nm; and ramsdellite, a Mn oxide, MnO_2, with peaks at 0.4072, 0.2553, 0.2438, 0.2422, 0.2344, 0.2147, 0.1906, 0.1660, and 0.1491 nm (Figure 3b and Table 1). The d spacings for the identified nsutite are similar to those described in the JCPDS-ICDD 17-0510 (Powder Diffraction File, Set 42, 1992), except for the absence of one medium (0.160 nm) and one weak peak (0.1305 nm) for the experimental sample (Table 1). For ramsdellite, the XRD patterns are almost identical to those described in the JCPDS-ICDD 39-0375. The crystal morphology of the newly-formed Mn minerals are shown in the electron micrograph (Figure 1b). Two types of crystals, fibrous crystals (F) and shuttle-shaped crystals (SS), roughly equal in proportion, were observed (Figure 1b). The shuttle-shaped crystal was most likely a nsutite; Tu (1993) showed the nsutite formed as shuttle-shaped cyrstals when birnessite was placed into 0.33 mol liter^{-1} $MnCl_2$ or $Mn(NO_3)_2$ solution.

At pH 4, a major proportion of the birnessite was transformed into cryptomelane, as seen from the XRD peaks at 0.698, 0.497, 0.484, 0.3149, 0.3110, 0.2399, 0.217, 0.1843, and 0.1654 nm (Figure 3c and Table 1). One medium-strong, one medium, and two weak peaks were missing as compared to those of cryptomelane-M, KMn_8O_{16} (JCPDS-ICDD 4-0778). In addition, a comparison of the experimental XRD data at 0.702, 0.494, 0.314, 0.2406, 0.216, and 0.1839 nm to those of manjiroite-M, $(Na,K)Mn_8O_{16}\cdot xH_2O$ (JCPDS-ICDD 21-1153), showed only one weak peak missing. The transmission micrograph of the experimental sample was similar to that shown by McKenzie (1989) for cryptomelane, which appeared as lath-shaped crystals. Also, the conversion of birnessite to cryptomelane has been achieved by several workers (Buser and Feitknecht, 1954; Gattow and Glemser, 1961; Glemser *et al.*, 1961) by directly igniting synthetic birnessite at 400°C or boiling birnessite that had been prewashed with $MnSO_4$ solution or dilute HCl. The lath-shaped crystals (CR in Figure 1c), about 0.4 μm in length, were most likely crymptomelane. Only trace amounts of two other Mn minerals could be distinguished in the electron micrograph as moss-like crystals (M) and the crystals (SS in Figure 1c) that appeared similar in shape to those observed at pH 2.4 (SS in Figure 1b).

The XRD patterns obtained from the products at pH 5 could not be matched with any Mn minerals filed in the most recent Powder Diffraction File database (PDF-2 on CD-ROM, Set 42) by the international Centre for Diffraction Data (ICDD). The electron micrograph showed that there were two kinds of crystals: rods (R) and hexagonal-cones (HC in Figure 1d). Owing to the lack of information on the XRD patterns and previous description of their morphology in the literature, their identification cannot be made using only X-ray data and TEM graphs at this point. The electron micrograph seemingly showed the presence of a third moss-like mineral at pH 5.

The hexagonal cones which occurred at pH 5, at first glance, appeared to be stacks of triangular plates. Careful study of the enlarged cone (Figure 1d, inset) revealed to us that it may have consisted of various sizes of cones in which cones of smaller diameter were stuck inside those of larger diameter—an unusual growth habit. In several cases, the separation of the cone layers along the cleavage was clearly observable. The rod-shaped crystals measured >1.2 μm in length, three times longer than the cryptomelane prepared by aging

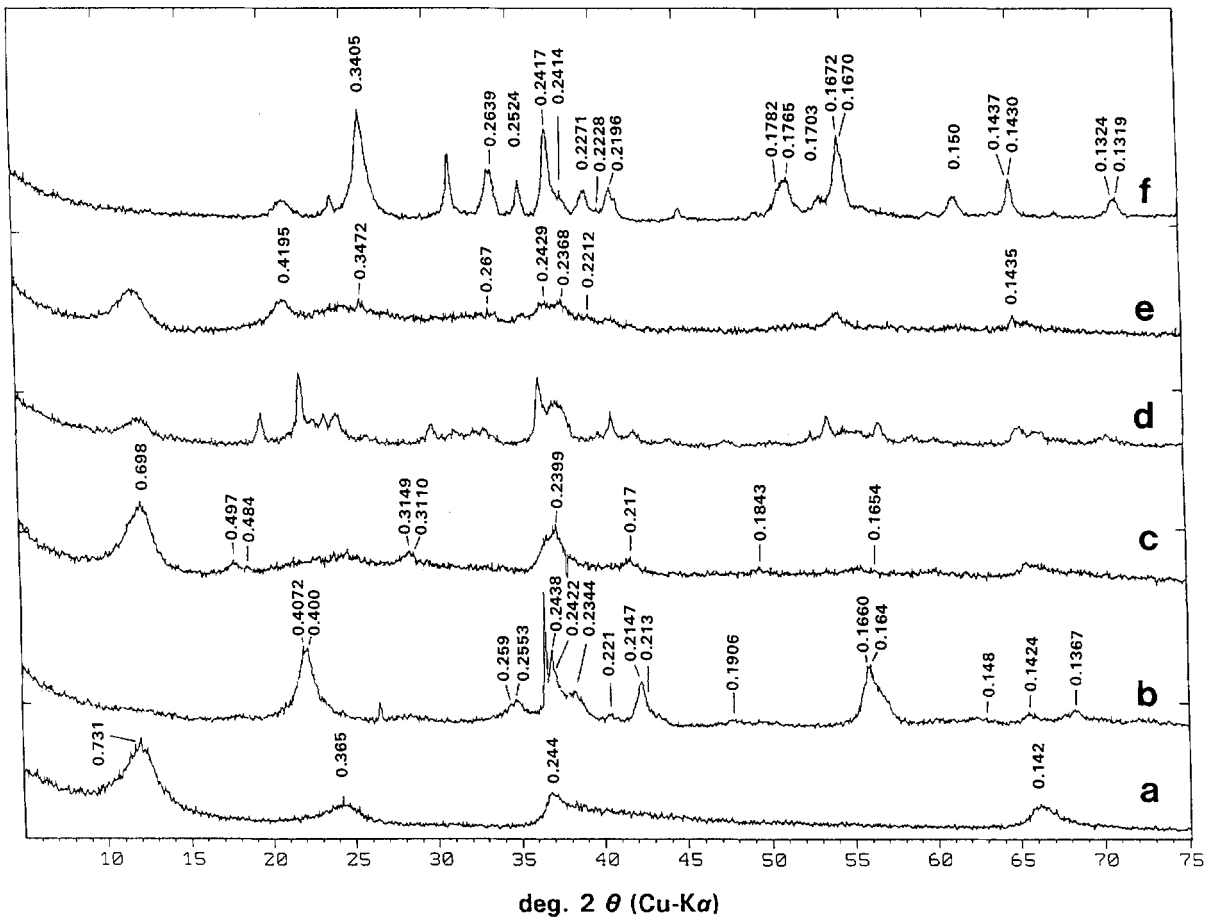

Figure 3. X-ray diffraction patterns of a) a synthetic birnessite and the products transformed from the birnessite after treatment with 0.33 mol liter^{-1} $MnSO_4$ solution at different pHs (b–f); b) pH 2.4, c) pH 4, d) pH 5, e) pH 6, and f) pH 8. The labeled peaks are identified.

birnessite in 0.33 mol liter^{-1} $MnSO_4$ at pH 4 (Figure 1c).

The products formed at pH 6 gave XRD patterns that indicated the presence of groutite, a α-MnOOH (JCPDS-ICDD 24-0713). The experimental sample lacked only one peak at 0.281 nm as compared with the standard groutite (Table 1). Two types of crystals were evidently distinguishable in the electron micrograph (Figure 1e): the hexagonal cones (HC) and parallel intergrowths of slat-shaped crystals (bundles of needles) (S). The needle-shaped mineral had a length similar to the fibrous crystals of ramsdellite formed at pH 2.4; but unlike the mineral, it occurred in bundles and seemed rigid so that broken pieces were commonly observable in the micrographs. Also unlike the rod-shaped mineral formed at pH 5, the crystals of this mineral were much shorter and thinner, resulting in increased transparency. Since the hexagonal cones occurred both at pH 5 and 6, which was not identified from the XRD data, and this needle-shaped phase formed only at pH 6, it can be inferred that these needles were groutite. The moss-like crystals, similar to those described at pH 4 and 5, were also observed in the micrograph at pH 6. The XRD data of the moss-like crystals resembled, more or less, its parent material (birnessite). This thus suggests that the moss-like material may be the intermediate of the transformation of birnessite to other Mn minerals at pH 4 to 6.

The XRD patterns obtained from the products at pH 8 indicate the formation of manganite (MnOOH) (JCPDS-ICDD 41-1379) with eight most intense peak lines positioned at 0.341, 0.264, 0.178, 0.2417, 0.1672, 0.2414, 0.1670, and 0.252 nm. Under the electron microscope, manganite appeared as short rod-shaped crystals <0.08 μm in length (Figure 1f, SR). The manganite formed at pH 8 was most likely a result of oxidation of $Mn(OH)_2$, which precipitated from the $MnSO_4$ solution during the process of pH adjustment

https://doi.org/10.1346/CCMN.1994.0420310 Published online by Cambridge University Press

Table 1. X-ray diffraction data and identified phases for the final products formed from birnessite after treatment with 0.33 mol L^{-1} $MnSO_4$ solution at different pH values.

Treatment	d spacings (nm) and intensities (%)												JCPDS card
pH 2.4	0.4250 (23)	0.4038 (62)	0.4003 (60)	0.3349 (23)	0.2601 (22)	0.2575 (25)	0.2456 (100)	0.2428 (59)	0.2346 (31)	0.2224 (15)	0.2132 (38)	0.2087 (15)	
	0.1898 (11)	0.1650 (36)	0.1642 (48)	0.1487 (13)	0.1423 (17)	0.1372 (19)							
Identified phases: Mn oxide hydroxide/Nsutite = $Mn(O, OH)_2$ Hexagonal a: 0.965 c: 0.443													17-0510
	0.400 (64)	0.259 (14)	0.242 (44)	0.233 (47)	0.221 (7)	0.213 (30)	0.207 (4)	0.190 (10)	0.164 (68)	⟨0.160⟩ ⟨30⟩	0.148 (17)	0.1424 (10)	
	0.1367 (27)	⟨0.1305⟩ ⟨14⟩											
Mn oxide/Ramsdellite = MnO_2 Orthorhombic a: 0.4533 b: 0.927 c: 0.443													39-0375
	0.4072 (64)	0.2553 (22)	0.2438 (17)	0.2422 (1)	0.2344 (17)	0.2147 (9)	0.1906 (10)	0.1660 (17)	0.1491 (1)				
pH 4.0	0.7161 (100)	0.4991 (40)	0.4750 (34)	0.3705 (48)	0.3585 (51)	0.3149 (50)	0.3125 (49)	0.2443 (64)	0.2402 (75)	0.2174 (40)	0.1954 (28)	0.1842 (33)	
	0.1651 (34)	0.1538 (31)	0.1423 (37)	0.1403 (34)									
Identified phases: Potassium Mn oxide/Cryptomelane = $K_2Mn_8O_{16}$ Monoclinic a: 0.979 b: 0.288 c: 0.994													4-0778
	0.698 (40)	0.497 (30)	0.484 (50)	0.3149 (30)	0.3110 (80)	⟨0.2481⟩ ⟨30⟩	0.2399 (100)	⟨0.2194⟩ ⟨40⟩	0.217 (30)	0.1843 (40)	⟨0.1820⟩ ⟨50⟩		
	0.1654 (80)	⟨0.1617⟩ ⟨70⟩											
Potassium sodium Mn oxide hydrate/Manjiroite = $(Na, K)Mn_8O_{16}\cdot xH_2O$ Hexagonal a: 0.965 c: 0.443													
	0.702 (69)	0.494 (55)	0.314 (66)	0.2406 (73)	0.216 (48)	0.1839 (33)	⟨0-.1548⟩ ⟨33⟩						
pH 5.0	0.7100 (49)	0.4493 (54)	0.4352 (26)	0.4151 (32)	0.4016 (100)	0.3889 (47)	0.3769 (53)	0.3653 (54)	0.3575 (36)	0.3425 (29)	0.3258 (25)	0.3146 (24)	
	0.2972 (41)	0.2949 (32)	0.2852 (34)	0.2748 (37)	0.2688 (35)	0.2460 (94)	0.2410 (67)	0.2386 (68)	0.2252 (32)	0.2210 (54)	0.2144 (34)	0.2041 (23)	
	0.1909 (23)	0.1735 (33)	0.1705 (49)	0.1678 (38)	0.1653 (33)	0.1620 (42)	0.1568 (29)	0.1533 (25)	0.1428 (39)	0.1409 (31)	0.1334 (20)	0.1325 (26)	
pH 6.0	0.8718 (69)	0.7219 (100)	0.4199 (84)	0.3606 (79)	0.3439 (85)	0.2665 (69)	0.2422 (80)	0.2369 (83)	0.2199 (59)	0.2152 (51)	0.1879 (42)	0.1681 (64)	0.1433 (58)
Identified phases: Mn hydroxide/Groutite = MnOOH Orthorhombic a: 0.456 b: 1.000 c: 0.287													24-0713
	0.4195 (142)	0.3472 (14)	⟨0.281⟩ ⟨48⟩	0.267 (41)	0.2429 (6)	0.2368 (68)	0.2212 (10)	0.1435 (9)					
pH 8.0	0.4166 (25)	0.3670 (28)	0.3418 (100)	0.3011 (13)	0.2851 (63)	0.2658 (50)	0.2641 (50)	0.2524 (40)	0.2413 (83)	0.2363 (31)	0.2280 (32)	0.2239 (17)	
	0.2199 (34)	0.2179 (25)	0.2008 (17)	0.1829 (14)	0.1800 (20)	0.1788 (32)	0.1771 (42)	0.1710 (26)	0.1677 (76)	0.1541 (13)	0.1505 (25)	0.1458 (12)	

Table 1. Continued.

Treatment	d spacings (nm) and intensities (%)											JCPDS card
	0.1436 (39)	0.1384 (12)	0.1324 (22)	0.1321 (24)								
Identified phases: Mn hydroxide/Manganite = MnOOH Monoclinic a: 0.530 b: 0.5278 c: 0.5307												41-1379
	0.3405 (220)	0.2639 (53)	0.2524 (26)	0.2417 (37)	0.2414 (35)	0.2271 (22)	0.2228 (4)	0.2196 (20)	0.1782 (46)	0.1765 (2)	0.1703 (22)	0.1672 (37)
	0.1670 (35)	⟨0.164⟩ ⟨20⟩	0.150 (20)	0.1437 (11)	0.1430 (11)	0.1324 (20)	0.1319 (11)					

( ) intensity of the XRD peak, ⟨ ⟩ missing peaks as compared to the mineral on JCPDS-ICDD card.

with NaOH. The longer rod-shaped crystals (Figure 1f, LR) transformed from birnessite, about 0.2 μm in length, were not identified by X-ray diffractometry.

Transformation of birnessite as affected by concentration of $MnSO_4$

The rate of alteration of birnessite to a new Mn mineral increased with an increase in concentration of Mn at a given pH. It took only 5 days for complete transformation of birnessite to manganite and another unidentified mineral at a concentration of 0.33 mol liter^{-1} $MnSO_4$ and a suspension pH 8 (Figure 4c), whereas no change of birnessite occurred at 0.0033 mol liter^{-1} $MnSO_4$ even after one month (Figure 4a). The XRD pattern obtained at 0.033 mol liter^{-1} $MnSO_4$ showed some new peaks as well as the presence of birnessite (Figure 4b).

Morphological changes of birnessite as affected by pH and reaction time

The TEM pictures in Figure 5 illustrate the sequential morphological alteration of the birnessite after treatment with 0.33 mol L^{-1} $MnSO_4$ at day 1, 3, and 5 (referred to as a–c at pH 2.4 and d–f at pH 6, respectively). At pH 2.4, the separation of some aggregates from birnessite was visible after reaction for 1 day. However, by day 3, formation of needle-shaped and shuttle-shaped crystals was observed. The transformation was close to completion by day 5. At pH 6, the rate of reaction was much faster than that at pH 2.4. The birnessite was reorientated or converted to fine fibrous crystals by day 1. After 3 days, the fine fibrous crystals changed to thicker separate needle crystals (bundles of fibers). After 5 days, both the hexagonal cones and needle-like crystals were clearly identifiable.

DISCUSSION

The results demonstrated that Mn^{2+} in solution acted both as a catalyst and essential component for the transformation of birnessite. The pH controlled the type of final products formed. Both the concentration of Mn^{2+} and pH determined the rate of the reaction.

The fate of Mn^{2+} scavenged by birnessite has interested researchers for years. Pankow and Morgan (1981) proposed that specific adsorption was responsible for the high affinity of Mn oxides for Mn^{2+}. A number of workers (Hem, 1963; Morgan and Stumm, 1964; Sung and Morgan, 1981) believed that the adsorbed Mn^{2+} was oxidized to Mn^{4+} through autocatalytic reaction by the oxide surfaces. The oxidation of adsorbed Mn^{2+} on the oxide surfaces was suggested by Murray and Dillard (1979), who, using X-ray photoelectron spectroscopy, were unable to detect any Mn^{2+} on the surface of birnessite after adsorption of Mn^{2+}. Whether the oxidation of Mn^{2+} occurred during, just prior to, or after adsorption remains an enigma. This has implications on which Mn ions (the +2 or higher oxi-

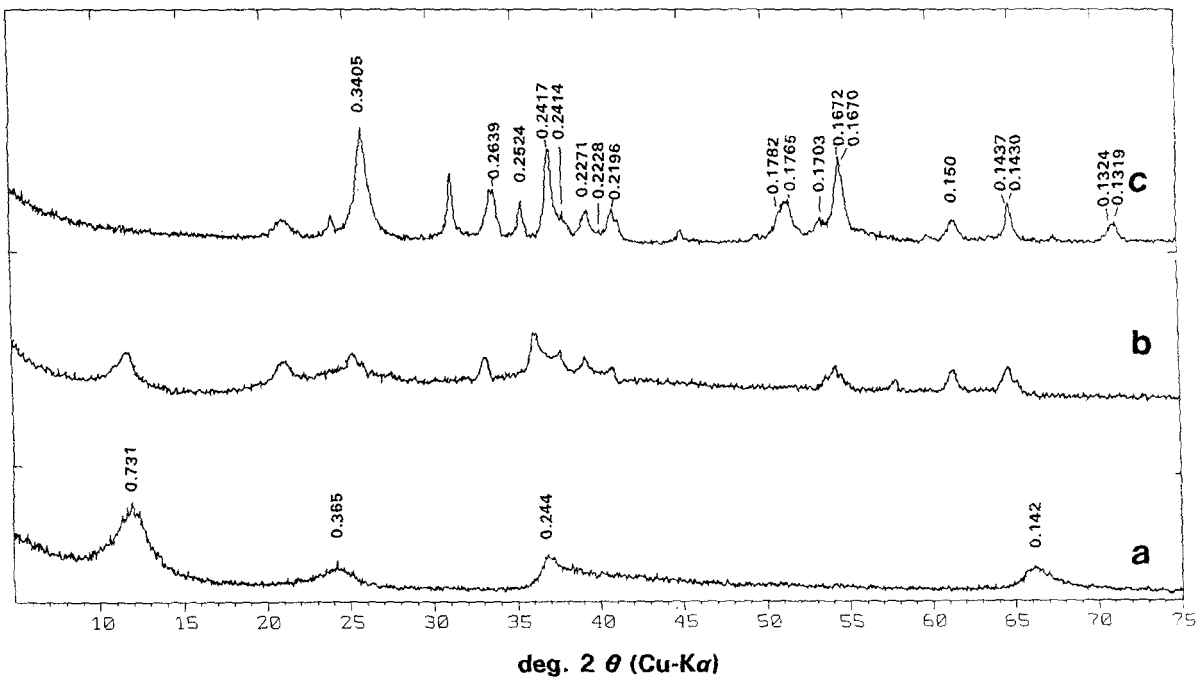

Figure 4. X-ray diffraction patterns of products formed after treatment of birnessite with solutions of a) 0.0033, b) 0.033 and c) 0.33 mol liter^{-1} $MnSO_4$ at pH 8.0. The labeled peaks are identified.

dation states) caused the structural change. There is no full answer at this time. However, we believe that Mn^{2+} ions played a major role in the structural transformations. In our study, it appeared that some, if not all, of the Mn^{2+} adsorbed were incorporated into the structure of the birnessite. The Mn^{2+} ions could have been included into the structure of birnessite, directly, by sorption from $MnSO_4$ solution. Alternatively, if oxidation had occurred during or prior to adsorption, the Mn^{4+} ions in the structure of birnessite would be the likely electron acceptor, being reduced to Mn^{2+} during the autocatalysis. In either case, Mn^{2+} was incorporated into the structure. The incorporation of Mn^{2+} into the structure would change the Mn-O bond length of birnessite and cause a charge imbalance. Feitknecht *et al.* (1960) suggested that the structure becomes unstable and rearranges to that of a new phase if a sufficient amount of Mn was incorporated into the structure. Therefore, it is most likely that incorporation of Mn^{2+} into the structure of birnessite subsequently induced spontaneous solid state rearrangement and reorientation of atoms in the birnessite crystal structure, leading to the transformation of birnessite into a series of new Mn minerals. Based on the X-ray identification, the major oxidation states of the identified phases were Mn^{4+} at pH 2.4 and 4 and Mn^{3+} at pH 6. This indicated that the Mn^{2+} ions retained by birnessite were eventually oxidized to Mn(III) and/or Mn(IV) as the transformation of new phases proceeded with time. This likely occurred using oxygen as the electron acceptor, since there was no other electron acceptor present in the system. It did not appear that the new minerals formed ex-solution either, since the appearance of the newly formed products was at the expense (i.e., disappearance) of birnessite. We were also unable to synthesize the same products at any pH with the exception of manganite at pH $\geq$ 7 when $MnSO_4$ solutions were aged alone, i.e., in the absence of birnessite. Finally, we did not observe any dissolution of the suspended birnessite followed by recrystallization or reprecipitation of new products. From the XRD and TEM data, the reaction with Mn^{2+} transformed birnessite from a relatively unstable and poorly crystallized mineral into more stable and highly crystallized products. This transformation virtually converts solution Mn^{2+} into an insoluble solid form in the structure of the newly formed minerals where Mn may exist in oxidation states from Mn(II) to Mn(IV).

CONCLUSIONS

Sorption of Mn^{2+} by birnessite at room temperature caused formation of new Mn phases. The final products of transformations were determined by solution pH and the rate of the transformation was determined by Mn^{2+} concentration and pH. Among phases that were crystalline by X-ray diffractometry, nsutite and ramsdellite were identified at pH 2.4, cryptomelane at pH 4, groutite at pH 6, and manganite at pH 8. The newly formed phases were the results of structural conversion

https://doi.org/10.1346/CCMN.1994.0420310 Published online by Cambridge University Press

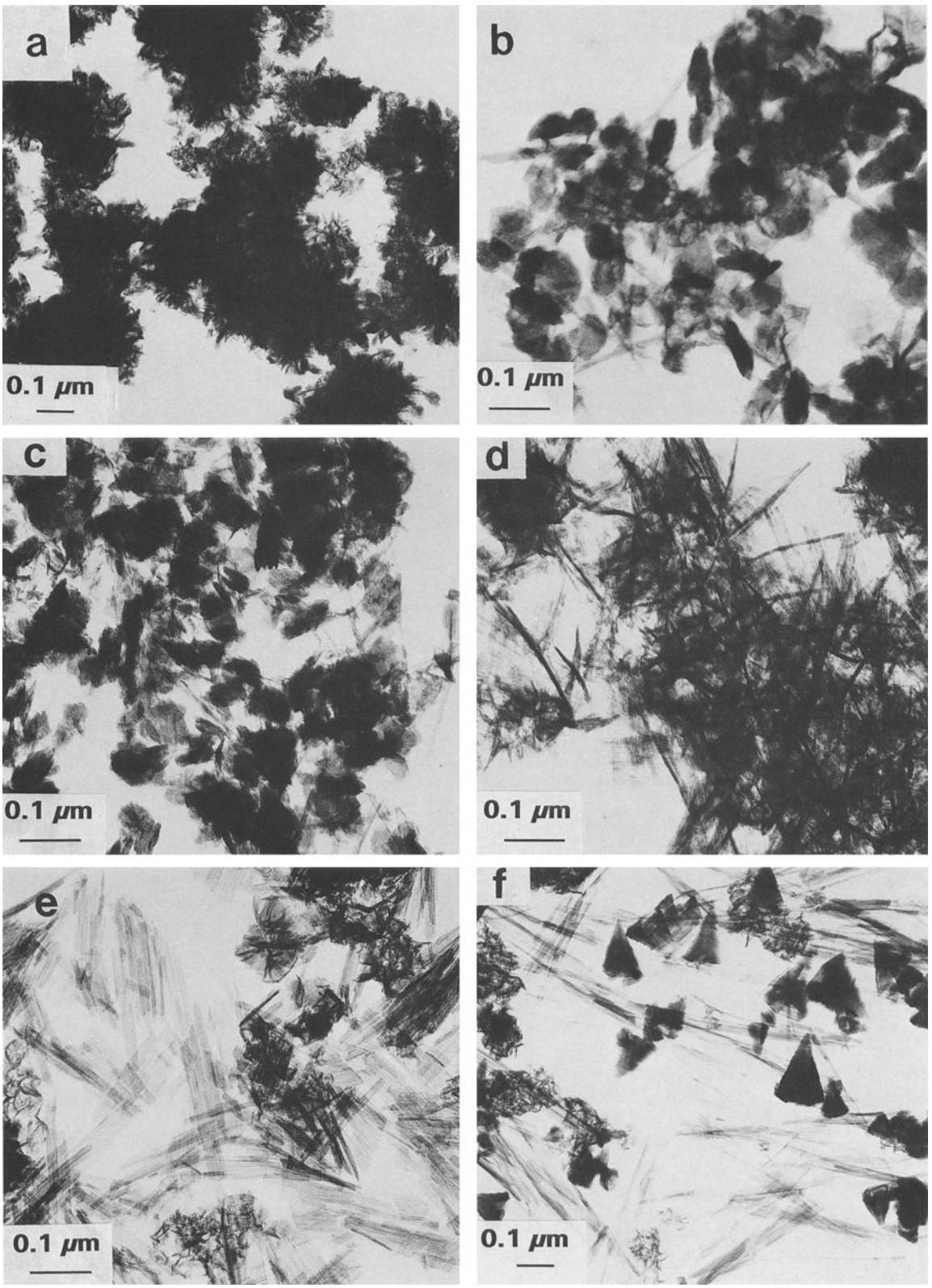

Figure 5. Sequential alteration of birnessite crystals accompanying new crystal formation as observed after treatment with 0.33 mol liter^{-1} $MnSO_4$ at pH 2.4 and 6.

https://doi.org/10.1346/CCMN.1994.0420310 Published online by Cambridge University Press

since dissolution of birnessite and reprecipitation of new phases were not observed.

This study provided new evidence that Mn^{2+} could induce transformation of birnessite to other new phases at room temperature. However, the chemistry of the transformation needs to be further investigated. Moreover, the oxidation states of the Mn in the new phases require further quantitative examination.

ACKNOWLEDGMENTS

The authors wish to thank the Potash and Phosphate Institute of Canada and the Natural Sciences and Engineering Research Council for their financial support, and the Agriculture Canada, Winnipeg Research Station, for use of their electron microscope facilities.

REFERENCES

Brown, F. H., Pabst, A., and Sawyer, D. L. (1971) Birnessite on colemanite at Boron, California: *Amer. Mineral.* **56,** 1057–1064.

Buser, W. P. and Feitknecht, W. (1954) Beitrag zur Kenntnis der Mangan(II)-manganite und des δ-MnO_2: *Helv. Chim. Acta* **37,** 2322–2333.

Davis, J. A. and D. B. Kent. (1990) Surface complexation modelling in aqueous geochemistry: in *Mineral-water Interface Geochemistry: Reviews in Mineralogy,* **23,** M. F. Hochella Jr. and A. F. White, eds., 177–260.

Feitknecht, W., Oswald, H. R., and Feitknecht-Steimann, V. (1960) Uber die topochemische einphasige reduktion von γ-MnO_2. *Helv. Chim. Acta.* **48,** 1947–1950.

Fendorf, S. E., Sparks, D. L., Franz, J. A., and Camaioni, D. M. (1993) Electron paramagnetic resonance stopped-flow kinetic study of manganese(II) sorption-desorption on birnessite: *Soil Sci. Soc. Am. J.* **57,** 57–62.

Frondel, O., Mervin, O. B., and Ito, J. (1960) New data on birnessite and hollandite: *Amer. Mineral.* **45,** 871–875.

Gattow, G. and Glemser, O. (1961) Darstellung und Eigenschaften von Braunstein. Part II: Die γ-and η-Gruppe der Brausteine: *Z. Anorg. Allg. Chem.* **309,** 20–36.

Glemser, O., Gattow, G., and Heisiek, H. (1961) Darstellung und Eigenschaften von Braunstein. Part I: Die δ-Gruppe der Brausteine: *Z. Anorg. Allg. Chem.* **309,** 1–19.

Golden, D. C., Dixon, J. B., and Cheng, C. C. (1986) Ion exchange, thermal transformations, and oxidizing properties of birnessite: *Clays & Clay Minerals* **34,** 511–520.

Healy, T. W., Herring, A. P., and Fuerstenau, D. W. (1966) The effect of crystal structure on the surface properties of a series of manganese dioxides: *J. Colloid Interface Sci.* **21,** 435–444.

Hem, J. D. (1963) Chemical equilibria and rates of manganese of oxidation: *US. Geol. Surv. Water Supply Paper* **1667-A.**

JCPDS—International Centre for Diffraction Data. (1992) Feint-Marquart's μPDSM micropowder diffraction search/match. Release 4.30. Pennsylvania, USA.

Jones, L. H. P. and Milne, A. A. (1956) Birnessite, a new manganese oxide mineral from Aberdeenshire, Scotland: *Mineral Mag.* **31,** 283–288.

Koljonen, T., Lahermo, P., and Garlson, L. (1976) Origin, mineralogy and geochemistry of manganese rocks and ferruginous precipitates found in sand graveldeposits in Finland: *Bull. Geol. Soc. Finland* **48,** 111–135.

Krauskopf, K. B. (1972) Geochemistry of micronutrients: in *Micronutrients in Agriculture,* J. J. Mortvedt, F. R. Cox, L. M. Shuman, and R. M. Walsh, eds., Soil Science Society of America, Madison, Wisconsin, 7–36.

McKenzie, R. M. (1971) The synthesis of birnessite, cryptomelane and some other oxides and hydroxides of manganese: *Mineral Mag.* **38,** 493–502.

McKenzie, R. M. (1980a). The adsorption of lead and other heavy metals on oxides of manganese and iron. *Aust. J. Soil Res.* **18,** 61–73.

McKenzie, R. M. (1980b) The manganese oxides in soils: in *Geology and Geochemistry of Manganese,* Vol. I, I. M. Varentsov and Gy Grasselly, eds., Hungarian Academy of Science, Budapest, 259–269.

McKenzie, R. M. (1981) The surface charge on manganese dioxide: *Aust. J. Soil. Sci. Res.* **19,** 41–50.

McKenzie, R. M. (1989) The manganese oxides and hydroxides: in *Minerals in Soil Environments,* J. B. Dixon and S. B. Weed, eds., Soil Science Society of America, Madison, Wisconsin, 439–465.

Morgan, J. J. and Stumm, W. (1964) The role of multivalent metal oxides in limnological transformations as exemplified by iron and manganese: *Adv. Water Pollut. Res., Proc. Int. Conf. 2nd. (Tokyo),* Pergamon Press, Oxford. 103–118.

Murray, J. W. and Dillard, J. G. (1979) The oxidation of cobalt(II) adsorbed on manganese oxide: *Geochim. Cosmochim. Acta.* **43,** 781–787.

Pankow, J. F. and Morgan, J. J. (1981) Kinetics for the aquatic environment: *Environmental Sci. and Tech,* **15,** 1306–1313.

Sung, W. and Morgan, J. J. (1981) Oxidative removal of Mn(II) from solution catalysed by the γ-FeOOH (lepidocrocite) surface: *Geochim. Cosmochim. Acta* **45,** 2377–2383.

Tu, S. (1993) Effects of KCl on solubility and bioavailability of Mn in soil and some reactions of birnessite in the presence of some Mn compounds. Ph.D. Dissertation, University of Manitoba, 112 pp.

(Received 2 March 1993; accepted 16 November 1993; Ms. 2341)